Designing robust crystallization processes in the presence of parameter uncertainty using attainable regions

Thomas Vetter,*,† Christopher L. Burcham,‡ and Michael F. Doherty¶

School of Chemical Engineering and Analytical Science, University of Manchester, Manchester M13 9 PL, United Kingdom, Small Molecule Design and Development, Eli Lilly & Company, Indianapolis, Indiana 46285, United States, and Department of Chemical Engineering, University of California, Santa Barbara, California 93106, United States

E-mail: thomas.vetter@manchester.ac.uk

Abstract

We consider the influence of uncertainty in crystallization kinetics (i.e., in the nucleation and growth rates) in the context of process design. Specifically, we model continuous and batch crystallization processes using population balance equation models and investigate how the inherent uncertainty in kinetic parameters propagates through the crystallization processes and how it ultimately affects the distribution of process outcomes (yield and mean particle size). We incorporate the effect of uncertainty into the concept of attainable regions, i.e., we exhaustively investigate which combinations of particle size and total residence time (or batch time) can be attained with a certain probability. Avoiding regions of low probability allows the design of robust crystallization processes that can deliver a product with desired specifications even when the original process was designed using inadequately characterized crystallization kinetics. The concepts presented in this article are illustrated by a case study on the cooling crystallization of paracetamol grown from ethanol as a solvent.

*To whom correspondence should be addressed

†School of Chemical Engineering and Analytical Science, University of Manchester, Manchester M13 9 PL, United Kingdom

‡Small Molecule Design and Development, Eli Lilly & Company, Indianapolis, Indiana 46285, United States

¶Department of Chemical Engineering, University of California, Santa Barbara, California 93106, United States

1 Introduction

Crystallization is widely applied in the manufacturing of particulate products with desired properties. Its popularity stems from the fact that it enables purification and a way to isolate the product in solid form. Crucially, crystallization also allows to tune physical product properties, such as the particle size distribution, which in turn affects downstream processes such as filtration and drying and determines the powder flowability of the product. Furthermore, the particle size distribution is often also a key factor in the performance of the product. One finds a plethora of examples for this observation, including such diverse areas as the manufacturing and lifetime of tungsten filaments in light bulbs, the color and brilliance of pigments[1] and the dissolution rate[2], bioavailability[3] and even the biocompatibility[4] of pharmaceutical products.

It is thus important to control or design crystallization processes to not only deliver the right purity, yield and crystal form, but also to produce crystals with a desired particle size distribution. Consequently, the design and control of crystallization processes have received considerable attention by the scientific community (see Nagy and Braatz[5] for a recent review). These studies can roughly be assigned to two classes: the calculation of optimal operating recipes[6–11] and feedback control strategies using various measurement tools to provide an estimate on the state of the process[12–15]. However, with a few notable exceptions[16–21], most studies have neglected uncertainties in the model structure, the crystallization kinetics and the operating recipe and have assumed that process disturbances are absent, thus failing to provide the necessary robustness. The influence of such uncertainties on the quality of the product crystals is well documented and can be considerable[22]. While it can be argued that process disturbances can be prevented or at least minimized, crystallization kinetics estimated from experimental data will always exhibit some degree of uncertainty[23], which can only be reduced when rather laborous characterization efforts are conducted. Clearly, a balance needs to be struck between an accurate characterization of crystallization kinetics and an acceptable level of uncertainty. However, to arrive at such a balance the uncertainty

needs to be either investigated experimentally or evaluated through appropriate models.

In this article we approach the problem of quantifying the effects of uncertainty from a process design perspective. Specifically, we investigate how uncertainty in the growth and nucleation rate parameters affects the outcome of optimal operating policies of continuous and (semi-)batch crystallizers that have been calculated using experimentally estimated parameter values, which are, however, only known within certain confidence intervals. Furthermore, we show that the attainable region approach, which we recently adapted to continuous and batch crystallization processes[24], can be used to design robust crystallization processes and to select crystallizer configurations that allow obtaining desired product characteristics with a high likelihood. The current trend towards continuous manufacturing processes in the pharmaceutical industry, which is likely to result in more "fit for purpose" crystallization process equipment in the future, is likely to increase the importance of such robust design strategies.

In the following, the process flowsheets and models considered in this article are presented in Section 2. In Section 3 we present an overview of possible sources of uncertainty in a crystallization process and introduce the Monte Carlo technique that will be used to sample the uncertainty contained in the crystallization kinetics. In Section 4 we extend the attainable region methodology to account for parameter uncertainty. Finally, in Section 5 we apply the presented techniques in a case study on the cooling crystalliztion of paracetamol grown from ethanol as the solvent.

2 Process flowsheets and models

In this article we consider three different types of crystallizers: cascades of mixed suspension mixed product removal crystallizers (MSMPRCs), semi-batch crystallizers and plug flow crystallizers (PFCs). The flowsheets and models are briefly introduced in this section. Additional considerations pertaining to the physical operation, advantages, pitfalls (and possible

remedies) of each processing strategy are provided in Sections 1 and 2 of our recent paper[24].

In the pharmaceutical industry crystallization processes are still mostly run as seeded or unseeded batch crystallizations. While a "seeding effect" could be achieved in continuous processes by recycling small particles from the product stream to the beginning of the PFC or the MSMPRC cascade, the use of recycle streams is currently not customary in the continuous production of APIs in the pharmaceutical industry. Hence, in order to enable a fair comparison between the process alternatives, we will exclude the possibility of introducing seed crystals to the semi-batch crystallizer and will only consider one pass MSMPRC cascades and one pass PFCs (i.e., no recycle). However, we point out that extending the presented process models and methodologies to seeded batch processes and continuous processes involving recycles could be accomplished if desired. We will also neglect the start-up behavior of the continuous processes, i.e., we only consider their performance once they have reached steady state. However, in all three cases we will allow the introduction of anti-solvent and cooling in order to create supersaturation and therefore induce crystallization. These process configurations can be described using the flowsheets shown in Figure 1, where the main variables describing the state of the process are the particle size distribution (n), the solute concentration (c), the temperature (T) and the anti-solvent weight fraction (a). The feed and product streams of the PFC and each MSMPRC are characterized by their volumetric flow rate (Q), their temperature and their solute and anti-solvent concentrations, as well as the particle size distribution they contain. The anti-solvent weight fraction in the i^{th} MSMPRC in a cascade is adjusted using the stream F_i, where F_i signifies a volumetric flow rate. Likewise, $F(t)$ signifies the anti-solvent addition stream to the semi-batch crystallizer. In the PFC the same kind of flexibility could be obtained through a differential sidestream $f(z)$, i.e., $f(z)$ signifies a volumetric flow rate per unit length. In practice however, the anti-solvent would be added to the PFC at specific points along its length coordinate. In the semi-batch this would be equivalent to instantaneoulsy adding a defined quantity of anti-solvent to the reactor at a specified time. Note that an MSMPRC cascade with an infinite

number of crystallizers is equivalent to a PFC when equivalent temperature and anti-solvent profiles are established and that the semi-batch crystallizer in time is equivalent to the PFC when batch time is converted to residence time in the PFC, just as in the case of chemical reactors (see for example Levenspiel[25]).

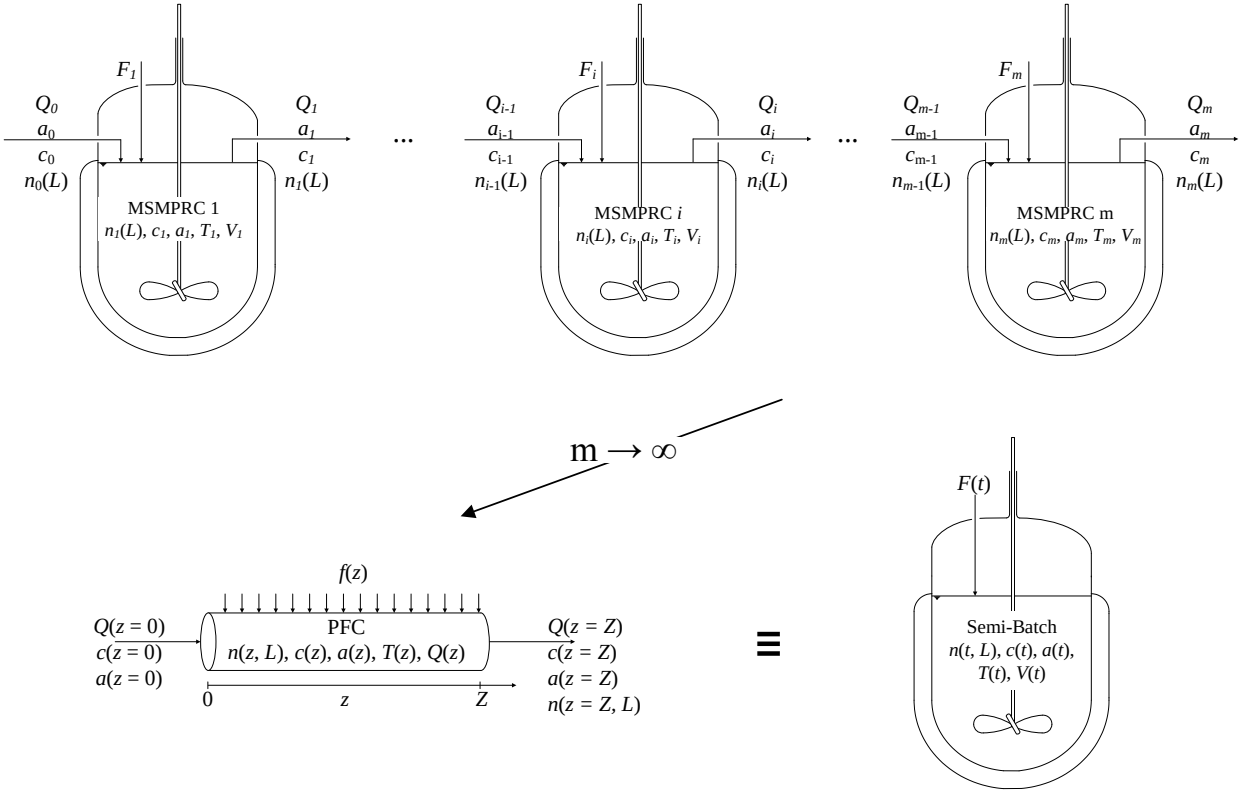

Figure 1: Flowsheet alternatives considered in this work: mixed suspension mixed product removal crystallizer (MSMPRC) cascade consisting of m MSMPRCs (top), plug flow crystallizer (PFC) with anti-solvent addition through a differential side stream (bottom left) and a semi-batch crystallizer with anti-solvent addition (bottom right).

In order to model these crystallization processes the population balance equation (PBE) framework[26,27] is used. In the following, we will assume that a number of ideality conditions applies to the crystallizers presented in Figure 1, which makes the model equations reasonably simple and fast to solve, thus enabling the developments presented later in this article. For the MSMPRC cascade, we assume that every MSMPRC

- is well-mixed,

- that all properties of the outflowing stream are identical to the conditions inside the respective MSMPRC,
- and that the mixture of solute, solvent and anti-solvent behaves as an ideal mixture.

We will further assume that nucleation and growth are the dominating mechanisms in the crystallization process, i.e., we will assume that all secondary processes (e.g., breakage and agglomeration of crystals) can be neglected and that the growth rate is independent of the crystal size. With these assumptions the PBE for the i^{th} MSMPRC in a cascade becomes

$$0 = -G\frac{\mathrm{d}n_i}{\mathrm{d}L} + \frac{Q_{i-1}n_{i-1} - Q_i n_i}{V_i} \tag{1}$$

where $n_i(L)$ is the number density distribution of the crystals so that $n_i \mathrm{d}L$ represents the number of crystals per suspension volume with sizes between L and $L + \mathrm{d}L$, G is the overall growth rate of the crystals, Q_i is the volumetric flow rate of the i^{th} stream and V_i is the volume of suspension. The boundary and regularity conditions for Eq. (1) are expressed as:

$$n_i(L = 0) = \frac{J}{G} \tag{2}$$

$$n_i(L = \infty) = 0 \tag{3}$$

where J is the nucleation rate. The growth and nucleation rate are dependent on the chemical potential difference between the crystalline and the liquid phase, which can be approximated by the supersaturation $S = c/c_\star$, where c is the solute concentration in the liquid phase and $c_\star(T, a)$ is the equilibrium solublity. Therefore, Eq. (1) is coupled with a mass balance (MB) for the solute:

$$0 = -3k_v\rho_c G \int_0^\infty L^2 n_i \, \mathrm{d}L + \frac{Q_{i-1}c_{i-1} - Q_i c_i}{V_i} \tag{4}$$

where k_v is the volumetric shape factor and ρ_c is the crystal density. Note that by (for example) specifying an overall production rate, as well as residence times, anti-solvent frac-

tions and temperatures for each crystallizer the flowrates of all streams and volumes of all crystallizers can be calculated. Similar PBEs and MBs can be derived for the PFC and the semi-batch crystallizer; we report these equations and some considerations pertaining to them in the Supporting Information (Appendix A).

In order to evaluate the model Eqs. (1) and (4) need to be solved simultaneously. The preferred method for this task depends on the form of the constitutive equations for nucleation and crystal growth (J and G, respectively). For the case study treated in this article the method of moments combined with analytical solutions for the steady state particle size distribution provide a computationally efficient option (see supporting material of Vetter et al.[24] for derivations).

3 Uncertainty analysis

3.1 Sources of uncertainty

Crystallization processes and the models describing them are subject to different kind of uncertainties, which will be categorized in the following way in this article:

- Structural uncertainty
- Measurement errors
- Parameter uncertainty
- Variability in operating conditions

Structural uncertainty is sometimes referred to as model bias, model inadequacy or model discrepancy and essentially stems from a lack of understanding of the underlying physics of a process, i.e., it is present when a model is chosen that does not fully describe the real process. For rather complicated processes such as crystallization, that we cannot (yet) entirely describe on a first principles basis, this type of uncertainty is always present. However, one

can formulate models with parameters that can be estimated by minimizing the difference of model outputs and experimental data (e.g., concentration profiles, particle size distributions, etc.), where the difference between model outputs and experimental data is quantified using an appropriate objective function. In the following, Φ is the objective function, $\mathbf{k}$ the vector of model parameters (containing N_k parameter values) and $\overline{\mathbf{k}}$ are the values of the model parameters at which Φ attains a minimum. The selection of an adequate model, i.e., a model that describes the experimental data well (low value of Φ), is often referred to as model identification and is discussed in detail elsewhere[28–30]. Due to the presence of unavoidable (random) measurement errors on the experimental data (i.e., white noise) one would expect $\Phi(\overline{\mathbf{k}}) > 0$ even for a perfect model. The parameter uncertainty refers to the precision with which $\overline{\mathbf{k}}$ can be estimated. It depends on the total amount of experimental data, the operating conditions at which the data were obtained and the amount of measurement noise. Assuming that the experimental data are of the same quality at all operating conditions, the parameter uncertainty can be reduced by providing more data in a large range of operating conditions or by reducing the amount of noise through the use of measurement techniques with higher precision and accuracy. Different ways to approximate the parameter uncertainty for the nonlinear models presented in Section 2 are reported in Bard[31], Caracotsios and Stewart[32], Donaldson and Schnabel[33]. Lastly, uncertainty can stem from variabilities in the operating conditions that are not accounted for in the model. For the crystallization processes and models in Section 2 fluctuations in any of the flow rates, in the composition of the feed stream or in any of the crystallizer temperatures are examples for this type of uncertainty.

In this article we focus exclusively on the effect of parameter uncertainty on product characteristics and will assume that structural uncertainty and variability in operating conditions are absent. Specifically, we will only consider uncertainty present in kinetic parameters (i.e., the parameters in the growth rate G and the nucleation rate J) and will assume that the thermodynamics of the system under investigation are well understood and known precisely,

which is a reasonable assumption since the relative uncertainty on kinetic parameters is typically orders of magnitude larger than for solubility measurements.

3.2 Description of parameter uncertainty

Once the parmeter uncertainty has been quantified, a hyperellipsoidal confidence region[17] can be established, which can be expressed as

$$\mathcal{C} = \left\{ \mathbf{k} \in \mathbb{R}^{N_k} \;\middle|\; \left(\mathbf{k} - \overline{\mathbf{k}}\right)^T \mathbf{V}_k \left(\mathbf{k} - \overline{\mathbf{k}}\right) \leq \chi^2_{N_k}(\alpha) \right\} \tag{5}$$

where $\mathbf{V}_k$ is the parameter covariance matrix, $\chi^2_{N_k}$ is the chi-squared distribution function with N_k degrees of freedom and α is the confidence level. The probability density distribution of the parameters is then a multivariate normal distribution:

$$g(\mathbf{k}) = \frac{1}{(2\pi)^{N_k/2} \left|\mathbf{V}_k\right|^{1/2}} \exp\left(-\frac{1}{2} \left(\mathbf{k} - \overline{\mathbf{k}}\right)^T \mathbf{V}_k^{-1} \left(\mathbf{k} - \overline{\mathbf{k}}\right) \right) \tag{6}$$

where $|\mathbf{V}_k|^{1/2}$ is the square root of the determinant of the positive semi-definite matrix $\mathbf{V}_k$. It follows from this description that $g(\overline{\mathbf{k}})$ is the maximum of this function for any covariance matrix $\mathbf{V}_k$ and if the parameters were perfectly known $g(\mathbf{k})$ becomes a Dirac delta distribution, i.e., $g(\mathbf{k}) = \delta(\mathbf{k} - \overline{\mathbf{k}})$. Note that reporting high-dimensional (when $N_k > 2$) confidence regions succinctly is difficult, so that confidence intervals on individual parameters are often the preferred method to describe parameter uncertainty. Conservative estimates of confidence intervals can be obtained by finding the box that circumscribes the hyperellipsoidal confidence region (Bard[31] describes several ways to accomplish this). It is often chosen to align the box in the parameter space, such that each of the sides is parallel to one of the parameter axes. Conservative confidence intervals can then be obtained as the lengths of the sides of this box, cf. Figure 2. Note that reporting confidence intervals in this way is equivalent to assuming that none of the parameters are correlated, which leads to a diagonal

covariance matrix $\mathbf{V}_k$. The elements on the diagonal of the matrix are then

$$(V_k)_{ii} = \left(\frac{\delta_i}{2t_{\alpha,\nu}}\right)^2 \tag{7}$$

where $t_{\alpha,\nu}$ is the quantile of Student's t-distribution with confidence level α and ν degrees of freedom.

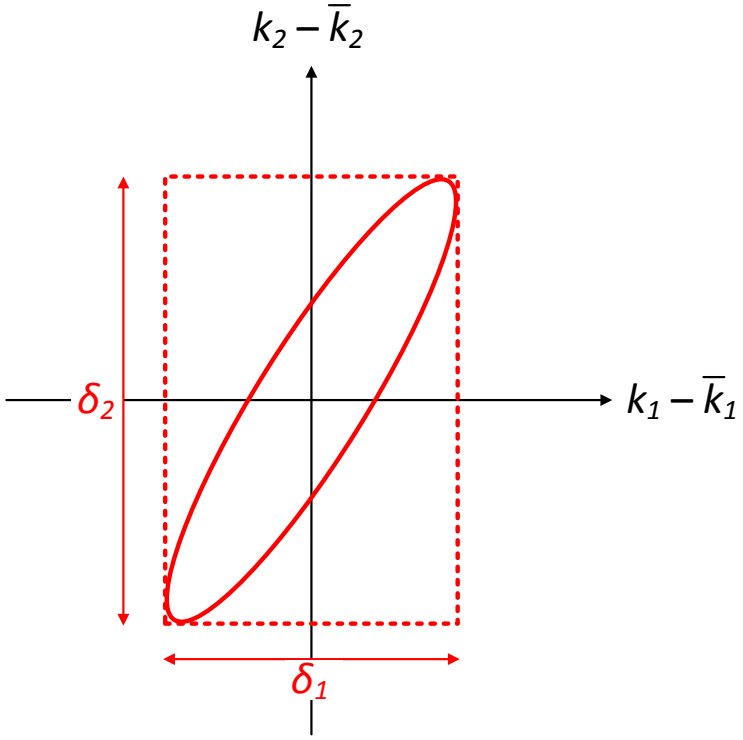

Figure 2: Conceptual depiction of the confidence region on mean centered parameter axes for a model with two parameters (solid line). Conservative confidence intervals can be obtained as the length and width of the box circumscribing the confidence region (dashed line). The width of the confidence interval for parameter k_i is shown as δ_i. Figure adapted from Rawlings et al.[23].

3.3 Quantifying output uncertainties

An intuitive way to sample the parameter uncertainty distribution is to perform Monte Carlo simulations, i.e., by taking N_s random samples from $g(\mathbf{k})$, leading to a $(N_s \times N_k)$ matrix of parameters. In our case we have taken the random samples from $g(\mathbf{k})$ using the

randn function available in MatLAB2014b. In order to evaluate how the parameter uncertainty propagates through the process, the crystallization process is simulated for each row of parameters, which leads to a distribution of process outcomes that can be subsequently evaluated. Hence, this analysis can provide a probability distribution for any process characteristic (yield, particle size distribution, etc.). In this article, we will assume that the two process and product characteristics we are interested in are the yield, Y, and the volume-weighted mean particle size, $\overline{L}$, at the end of the crystallization process, i.e., in the m^{th} MSMPRC of a cascade. The yield is defined as

$$Y = \frac{Q_0 c_0 - Q_m c_m}{Q_0 c_0 - Q_f c_{\star,f}} \tag{8}$$

where $c_{\star,f}(T_f, a_f)$ is the solubility at the temperature and anti-solvent fraction at the end point of the crystallization process and Q_f is the flow rate that needs to be maintained in order to reach these conditions. The volume-weighted mean particle size is defined as

$$\overline{L} = \frac{\mu_4}{\mu_3} \tag{9}$$

where μ_j is the j^{th} moment of the particle size distribution in the last crystallizer of the cascade, defined as

$$\mu_j = \int_0^\infty L^j n_m \, \mathrm{d}L \tag{10}$$

While we have written Eqs. (8) to (10) with a cascade of m MSMPRCs in mind, they are easily adapted to the PFC or semi-batch crystallizer. The distribution of the yield and the mean particle size due to parameter uncertainty can be described through the corresponding probability density functions p_Y and $p_{\overline{L}}$. A crystallization process is typically designed to reach at least a desired yield Y_d. However, we appreciate the presence of uncertainty and therefore specify a tolerance ϵ_Y on the yield specification. One would then consider all process outcomes giving a yield of at least $Y_d - \epsilon_Y$ to be within the specifications. The

fraction of process outcomes that fulfill the yield specifications, P_Y, is therefore expressed as

$$P_Y = \int_{Y_d-\epsilon_Y}^{1} p_Y \, \mathrm{d}Y \tag{11}$$

The design specification for the mean particle size on the other hand is typically given as an interval around a desired mean particle size $\overline{L}_d$. Defining the lower tolerance and the upper tolerance on the desired particle size as $\epsilon_{\overline{L},\ell}$ and $\epsilon_{\overline{L},h}$, respectively, the fraction of process outcomes that fulfills the size specification, $P_{\overline{L}}$, can be calculated as

$$P_{\overline{L}} = \int_{\overline{L}_d-\epsilon_{\overline{L},\ell}}^{\overline{L}_d+\epsilon_{\overline{L},h}} p_{\overline{L}} \, \mathrm{d}\overline{L} \tag{12}$$

Note that P_Y and $P_{\overline{L}}$ not only depend on the parameter uncertainty, but also on the specific operating policy that was implemented to reach the yield and mean particle size specifications in a given crystallizer configuration. While it is straightforward to say that the fraction of process outcomes that fulfill the specifications will increase when the uncertainty in all kinetic parameters is decreased, one cannot predict a priori which operating policy is affected more by uncertainty in specific kinetic parameters. In fact, for some operating policies P_Y and $P_{\overline{L}}$ might depend more strongly on the uncertainty in the nucleation rate parameters than on the uncertainty in the growth rate parameters, while for other operating policies the reverse behavior could be observed. These interdependencies are investigated for the case of the cooling crystallization of paracetamol grown from ethanol for selected operating policies and equipment configurations in Section 5.2.

Note that there are also methods that are computationally more efficient (but less intuitive) than the Monte Carlo technique mentioned above, such as power series and polynomial chaos expansions[34]. These methods should be employed if the complexity (and therefore the computational burden) of the process model is high and/or if process outcomes with a low probability need to be characterized accurately. For the purposes of this article, we deemed

the performance of the Monte Carlo technique satisfactory.

4 Attainable regions for crystallization processes

In a seminal paper Horn[35] introduced the notion of attainable regions to the process design of chemical reactors. The attainable regions defined by Horn consisted of all possible outcome states of a system of chemical reactors including mixing of streams before and after reactors (i.e., all possible vectors of chemical composition at the end of a chemical reaction process) with the only knowledge required to find such regions being the chemical reaction network, the kinetics involved in it and the feed composition. After this initial contribution Glasser et al.[36] and Hildebrandt et al.[37] used geometric considerations to show that attainable regions for systems of ideal reactors and mixers are always convex. The approach was subsequently also applied to systems of reactors, mixers and separators[38,39]. The methodology and its limitations have been summarized by Feinberg[40] and Tang and Feinberg[41].

A modified attainable region approach can also be applied to particulate processes,[42] e.g., Raikar[43] has applied the approach to droplet size distributions in emulsions. We have recently shown that the attainable region concept can also be applied to process and product characteristics of continuous and batch crystallization processes[24]. In that paper we successfully identified two-dimensional attainable regions in a plane of mean crystal size versus total residence time for the three crystallizer configurations shown in Figure 1. Such attainable regions provide a convenient way to analyze the tradeoff between the ability to achieve a desired particle size, the overall productivity of the process (in terms of mass of product per unit time per process volume) and the capital cost required for a certain crystallizer configuration (provided equipment costing information is available).

However, to the best of our knowledge, attainable regions were never established for cases where significant parameter uncertainty is present, i.e., in the above studies the kinetic parameters were assumed to be precisely known (which is not possible for real systems,

cf. Section 3). In this article, we try to remedy this by introducing uncertainty-adjusted attainable regions: these regions allow us to judge with what confidence we are able to reach a certain point in a plane of mean particle size vs. total residence time, given that the kinetic parameters are only known to lie within certain confidence intervals. The methodology to obtain attainable regions for crystallization processes with known parameters will be summarized briefly in the following (Section 4.1) and will then be extended to cases where parameter uncertainty is present (Section 4.2).

4.1 Attainable regions for known parameters

In the following, we describe the methodology to find attainable regions in a plane of mean particle size versus total residence time for a given crystallizer configuration, i.e., for an MSMPRC cascade (with varying number of crystallizers), a PFC or a semi-batch crystallizer. In order to obtain economically meaningful processes a yield constraint $Y \geq Y_d$ (with Y defined as in Eq. (8)) is enforced. Enforcing a stringent constraint on the desired yield entails that process configurations at a given crystallizer volume result in production rates between $Y_d P$ and P, where P is a specified production rate (in mass per time). Clearly, the more stringent the yield constraint, the narrower the interval of obtained production rates. However, the size of the product particles, $\overline{L}$, resulting from these process configurations might be completely different due to different temperatures and anti-solvent fractions in the crystallizers and a different distribution of residence times along the cascade. It is therefore instructive to explore attainable regions in the plane of mean particle size versus total residence time. We have shown in Vetter et al.[24] that the boundaries of such an attainable region for a cascade of m MSMPRCs can be found by solving optimization problems that strive to minimize or maximize the mean particle size for a given total residence time by varying the residence times (τ_i), temperatures (T_i) and anti-solvent fractions (a_i) in each

crystallizer:

$$
\begin{aligned}
&\underset{T_i, a_i, \tau_i}{\text{minimize/maximize}} && \overline{L} \\
&\text{subject to} && \sum_{i=1}^{m} \tau_i = \tau \\
& && T_i \leq T_{i-1}, \\
& && a_i \geq a_{i-1}, \\
& && T_i \geq T_f, \\
& && a_i \leq a_f, \\
& && Y \geq Y_d.
\end{aligned}
\tag{13}
$$

where $i = 1, \ldots, m$, $\tau_i = Q_i/V_i$ is the residence time in the i^{th} crystallizer and τ is the sum of all residence times in the crystallizer, i.e., the total residence time in the crystallization process. We have also placed additional constraints on Eq. (13). Constraint 2 and 3 ensure that the temperature along the MSMPRC cascade decreases monotonically and that the anti-solvent fraction increases monotonically. Hence, cycles of growth and dissolution are not considered in this article. Constraints 4 and 5 represent a lower bound for the temperature and an upper bound for the anti-solvent fraction that are typically given by limitations on the cooling utilities and by considerations based on the phase diagram of the system (such as impurity rejection and solubility). Finding a direct analytical expression for the boundary of the attainable region is challenging since the underlying model equations (cf. Section 2) are nonlinear, however, by solving the optimization problems in Eq. (13) for different total residence times one is able to find smooth boundaries for the attainable region. Note that we could consider a different product characteristic than the mean particle size for the optimization target or add additional ones.[44]). Furthermore, equivalent versions of Eq. (13) can be written for the PFC and the semi-batch crystallizer by adjusting the definitions of Y, $\overline{L}$ and τ.

Knowing the boundaries of the attainable region, it is possible to find operating policies for points that give a desired mean particle size $\overline{L}_d$ by considering combinations of (τ, $\overline{L}$)

that lie within the attainable region. To this end, we formulate an optimization problem that minimizes the squared distance between the desired mean particle size $\overline{L}_d$ and the mean particle size that is obtained from a given operating policy, i.e., we write:

$$\begin{aligned} \underset{T_i, a_i, \tau_i}{\text{minimize}} \quad & \left(\overline{L} - \overline{L}_d\right)^2 \\ \text{subject to} \quad & \sum_{i=1}^{m} \tau_i = \tau \\ & T_i \leq T_{i-1}, \\ & a_i \geq a_{i-1}, \\ & T_i \geq T_f, \\ & a_i \leq a_f, \\ & Y \geq Y_d. \end{aligned} \tag{14}$$

In the cases that we considered in Vetter et al.[24] we found that the objective function $\left(\overline{L} - \overline{L}_d\right)^2$ can typically be minimized to values of the order of $10^{-6}\mu\text{m}^2$, i.e., for all practical purposes the desired particle size can be reached accurately and the attainable regions can be fully traversed.

4.2 Attainable regions in the presence of parameter uncertainty

The attainable region approach described above does not contain any information about parameter uncertainty; it predicts that all the points in the attainable region can be reached with full confidence. Unfortunately, kinetic parameters can only be estimated to a finite precision. It is instructive to know how strongly the attainable region depends on the inherently present parameter uncertainty. In order to quantify this effect the Monte Carlo approach described in Section 3.3 is used. We calculate the boundaries of attainable regions for all N_s parameter sets that have been sampled from the probability density function $g(\mathbf{k})$ (cf. Eq. (6)). The number of attainable regions that contain the point $(\overline{L}_d,\, \tau)$ divided by

N_s then gives the uncertainty-adjusted probability $p(\overline{L}, \tau)$ that this point can be reached. By calculating this probability for all points in the ($\overline{L}$, τ) plane, we get the uncertainty-adjusted attainable region for a given crystallizer configuration. If the kinetic parameters are precisley known to be $\overline{\mathbf{k}}$ (i.e., the widths of all parameter confidence intervals are zero: $\delta_i = 0 \; \forall \; i$), the uncertainty-adjusted attainable region is simply the original attainable region in which all points can be reached. Conversely, the larger the parameter uncertainty, the more diffuse the uncertainty-adjusted attainable region is expected to be. Furthermore, we expect the sensitivity of the attainable regions on parameter uncertainty to be different for different crystallizer configurations. The uncertainty-adjusted attainable regions for MSMPRC cascades with different numbers of crystallizers, semi-batch crystallizers and PFCs are considered in Section 5.4. The influence the widths of the parameter confidence intervals have on the size of the uncertainty-adjusted attainable region, is also discussed.

5 Results and discussion

5.1 Introduction of the case study

To establish the previously mentioned case study, knowledge of the crystallization kinetics, process start and end points, as well as product specifications are necessary. The crystallization kinetics pertaining to this model system have been investigated in several papers. The growth kinetics and solubility have been reported by Mitchell et al.[45] using seeded batch desupersaturation experiments. The primary nucleation kinetics were investigated in Mitchell et al.[46] using induction time experiments. The secondary nucleation kinetics were reported in Frawley et al.[47] using batch desupersaturation experiments at higher stirring rates. The kinetic expressions, kinetics parameters, solubility curve and other relevant physical constants are reported in Table 1. In the case of the primary and secondary nucleation kinetics 95% confidence intervals around the estimated values of the parameters (k_4 to k_7 in Table 1) were reported[46,47]. Unfortunately, the confidence intervals for the growth rate

parameters (k_1 to k_3 in Table 1) were not reported in the same fashion. In order to also investigate the effect of uncertainty in the growth kinetics, we will assume that the 95% confidence intervals of these parameters have a width of 20% of the respective estimated parameter values, which is in line with those reported for substances such as S-Mandelic acid and the racemate of Ibuprofen where the growth kinetics have been characterized extensively[48,49]. Consequently, the analysis that follows should be seen as a proof of methodology using reported kinetic parameters for the paracetamol/ethanol system with estimates for uncertainty around these parameters, where such estimates were provided and supplemented by realistic guesses (originating from other substances) for the parameters where information on parameter uncertainty was not provided in the original experimental papers on the paracetamol/ethanol system. Note that full parameter covariance matrices cannot be reconstructed from the reported confidence intervals alone, so that the covariance matrix $\mathbf{V}_k$ in Eq. (6) becomes a diagonal matrix, whose elements can be calculated from the confidence intervals using Eq. (7). Note that this is equivalent to say that the parameters were assumed to be uncorrelated in the experimental papers[45–47].

The start point of a crystallization process is typically given by the end point of the previous unit operation and is therefore fixed. The end point of the crystallization process on the other hand is rather flexible and is typically chosen to maximize the fraction of recovered solute, which depends on the phase diagram of the system. However, additional considerations, such as minimum and maximum allowable suspension density in the crystallizer and equipment capabilities, as well as the need for impurity rejection, additionally limit the choice of the end point. For the case study presented here, we have chosen start and end points that we considered to be reasonable, as detailed in Table 2. For the sake of example, we will consider two different mean size specifications for the product particles; $\overline{L}_d = 200$ μm (case I) and $\overline{L}_d = 400$ μm (case II) for the product particles. In both cases we will set a tolerance of 5% on the mean particle size (i.e., $\epsilon_{\overline{L},\ell} = \epsilon_{\overline{L},h} = 10$ μm for case I and $\epsilon_{\overline{L},\ell} = \epsilon_{\overline{L},h} = 20$ μm for case II) and a yield tolerance of 1% (i.e., $\epsilon_Y = 0.01$). All process and

Table 1: Substance data used in the case study [a]

crystalization type	cooling
solute	paracetamol
solvent	ethanol
solubility [b]	$c_\star = 0.2331 \exp(0.02179T)$
crystal growth [c]	$G = k_1 \exp\left(-\frac{k_2}{T}\right) \left(\frac{c-c_\star}{M}\right)^{k_3}$
	$k_1 \quad 9.979 \pm 0.998$ m$^{-3k_3+1}$ s^{-1} kmol^{k_3}
	$k_2 \quad (4.878 \pm 0.488) \times 10^3$ K
	$k_3 \quad 1.602 \pm 0.160$
primary nucleation [d]	$J_{\text{prim}} = k_4 \left(\frac{c-c_\star}{\rho_s}\right)^{k_5}$
	$k_4 \quad (2.662 \pm 1.678) \times 10^8$ m^{-3} s^{-1}
	$k_5 \quad 2.276 \pm 1.694$
secondary nucleation [e]	$J_{\text{sec}} = k_6 (c - c_\star)^{k_7} \mu_2$
	$k_6 \quad (2.656 \pm 0.102) \times 10^7$ m^{-2} s^{-1}
	$k_7 \quad 2.232 \pm 0.086$
shape factor, k_v	0.866
crystal density, ρ_c	1332 kg m^{-3}

[a] All expressions made consistent with the nomenclature in this paper, such that the same kinetic rates as in the original papers result; conversion factors introduced where necessary ($M = 151.17$ kg kmol^{-1}, $\rho_s = 789$ kg m^{-3}); note that $J = J_{\text{prim}} + J_{\text{sec}}$.

[b] Solubility data taken from Mitchell et al.[45].

[c] Parameters taken from Mitchell et al.[45]. The width of the confidence intervals on the growth rate parameters were assumed to be 20% of the respective parameter values.

[d] Parameters and confidence intervals taken from Mitchell et al.[46].

[e] Parameters and confidence intervals taken from Frawley et al.[47].

product specifications are summarized in Table 2.

For the above-mentioned case study, we have reported attainable regions for cascades consisting of different numbers of MSMPRCs, as well as for batch and plug flow crystallizers[24]. These attainable regions were calculated with the mean parameter values $\overline{\mathbf{k}}$ reported in Table 1. For example, we report the attainable regions for a cascade of three MSMPRCs and for the batch/plug flow crystallizers in Figure 3 as the solid green and solid blue line, respectively. The size specifications are drawn in this figure as horizontal dashed lines at 200 and 400 μm. For total residence times for which these lines lie within the attainable region of the MSMPRC cascade or the batch/PFC, an operating policy can be found that fulfills all constraints detailed in Eq. (14) and reaches the specified mean product particle sizes of 200 or 400 μm. In order to consider a specific example and investigate how parameter uncertainty affects process outcomes, we select a total residence time $\tau = 2.75$ h. As can be seen from Figure 3, both operating points (marked by a circle and diamond symbol) lie within the attainable region of the cascade consisting of three MSMPRCs as well as in the attainable region of the batch/PFC. The specific operating policies are discussed in detail in Appendix B in the Supporting Information.

Table 2: Process and product specifications

start temperature, T_0 [K]	341
end temperature, T_f [K]	273
start solubility, $c_\star(T_0)$ [kg m^{-3}]	396
end solubility, $c_\star(T_f)$ [kg m^{-3}]	89
desired yield, Y_d [-]	0.98
yield tolerance, ϵ_Y [-]	0.01
desired mean product particle size (case I), $\overline{L}_d$ [μm]	200
upper and lower size tolerance (case I), $\epsilon_{\overline{L},\ell}$, $\epsilon_{\overline{L},h}$ [μm]	10
desired mean product particle size (case II), $\overline{L}_d$ [μm]	400
upper and lower size tolerance (case II), $\epsilon_{\overline{L},\ell}$, $\epsilon_{\overline{L},h}$ [μm]	20
total residence time, τ [hours]	2.75

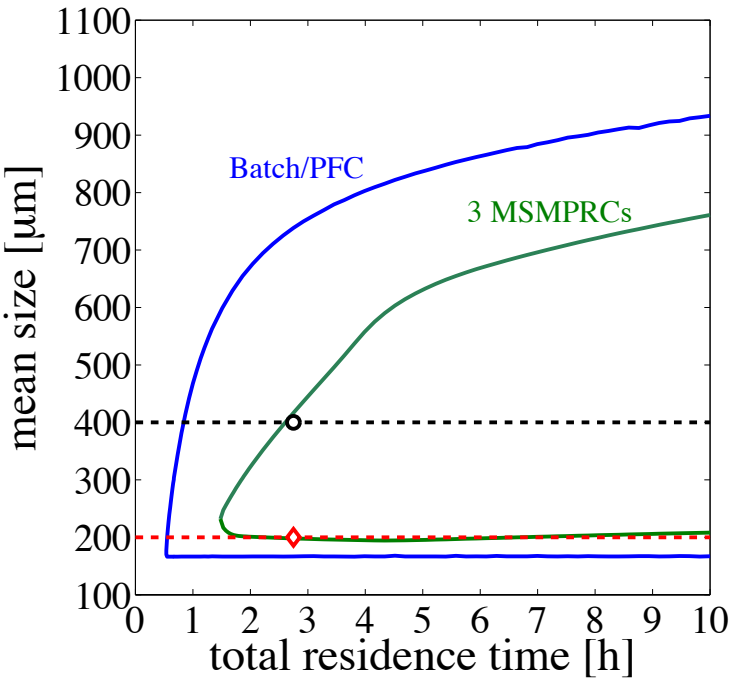

Figure 3: Attainable regions, specifications and selected operating points for a cascade of 3 MSMPRCs, as well as for the batch/PFC case. The solid lines represent the attainable regions, the dashed lines the particle size specifications and the symbols the selected operating points for the two particle size specifications.

5.2 Distribution of process outcomes

The propagation of uncertainty through the crystallization process is investigated using the Monte Carlo approach described in Section 3.3. We implement the operating policies calculated for the case studies in Table 2 for all N_s parameter sets that we sampled from the probability density distribution $g(\mathbf{k})$. For the purpose of this analysis we used $N_s = 5,000$ samples in order to obtain smooth distributions for p_Y and $p_{\overline{L}}$. The results are shown in Figure 4 where the upper two figures (Figures 4a and 4b) show the results for the MSMPRC cascade with three crystallizers and the bottom two subfigures (Figures 4c and 4d) show the results for the batch/PFC case. In these figures the red solid lines represent the probability density distributions p_Y and $p_{\overline{L}}$ for the operating policies designed to yield particles of mean size 200 μm, while the black solid lines represent the equivalent distributions for the operating policies designed to yield particles with 400 μm mean size. The dashed and dotted lines represent the desired specifications and their tolerances as defined in Table 2. When the majority of the distributions p_Y and $p_{\overline{L}}$ lie within the dotted lines of the same color, the operating policy yields a large fraction of process outcomes that are within the specifications. Formally, the fraction of in-spec process outcomes can be calculated using Eqs. (11) and (12). Figures 4a and 4c indicate that, due to uncertainty in the kinetic parameters, a large fraction of process outcomes lie outside the respective specifications, which suggests that uncertainty in the kinetic parameters should not be neglected when designing the crystallization process. It is noteworthy that neither the batch/PFC, nor the cascade of three MSMPRCs perform satisfactorily, i.e., the type of crystallizer used has only a small influence on the width of the distributions of process outcomes, so that improvements can only be achieved with a more precise characterization of the crystallization kinetics, i.e., with tighter confidence intervals around the kinetic parameters.

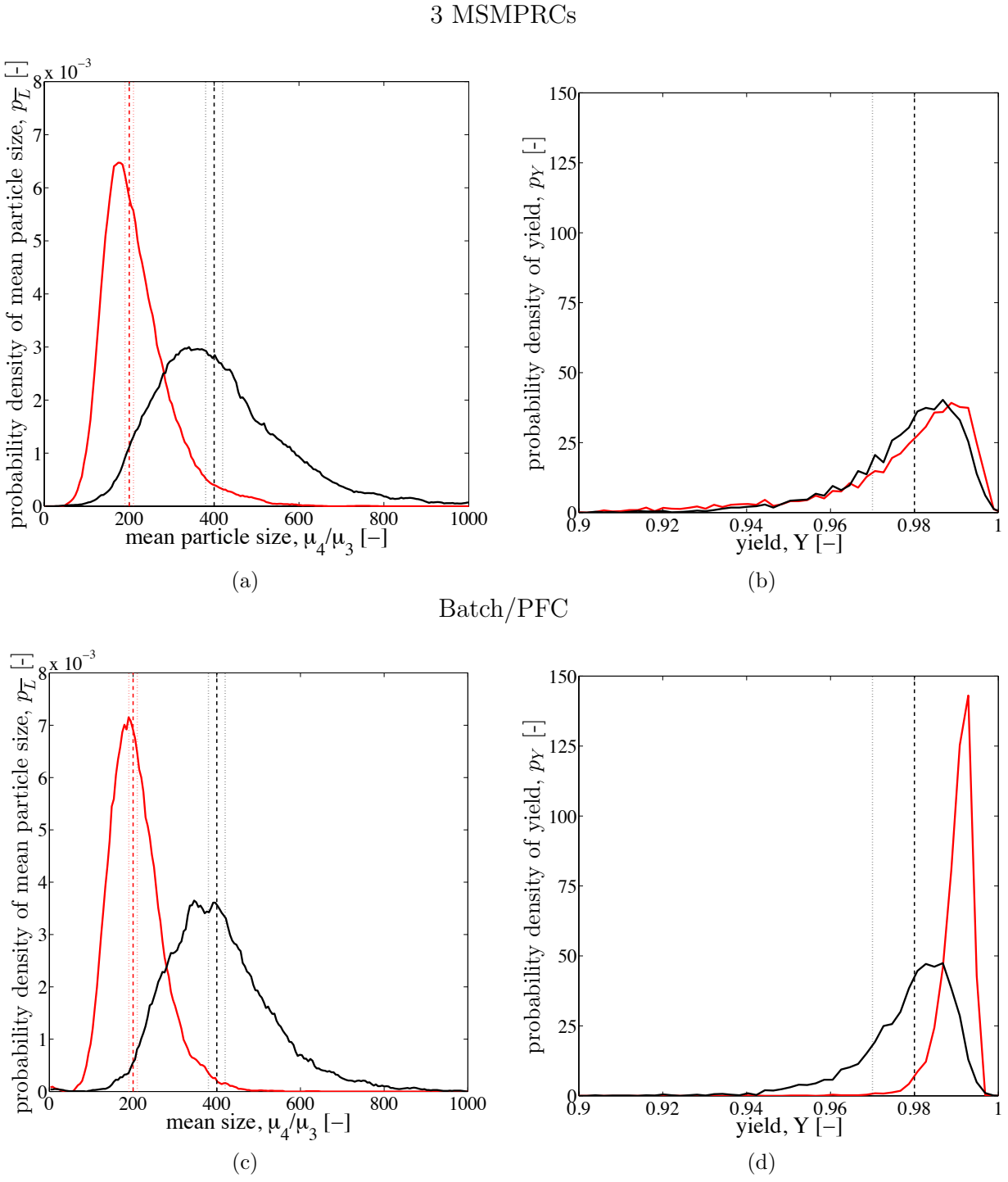

Figure 4: Distribution of process outcomes for specifications listed in Table 2. (a) and (b): size and yield for a cascade of three MSMPRCs, (c) and (d): size and yield for batch/PFC case.

5.3 Effect of confidence intervals on the distribution of process outcomes

In the following we investigate how much the fraction of "in spec" process outcomes increases when the confidence intervals, δ_i, around the mean parameter values $\overline{k}_i$ are reduced. Recall that experimental procedues are typically either designed to provide information about the growth kinetics (e.g., using seeded desupersaturation experiments) or to provide information about the nucleation kinetics (e.g., using induction time experiments or metastable zone width experiments). Clearly, we would like to know which type of experimental procedure has the greatest potential to narrow the distribution of process outcomes in the given case study. We will try to ellucidate this by assuming that we can shrink the confidence intervals of the kinetic parameters in the growth rate (k_1–k_3) and the nucleation rate (k_4–k_7) by the same factor. We thus define H_g and H_n as the ratio between newly shrunk confidence intervals ($\delta_{\text{new},i}$) and original confidence intervals ($\delta_{\text{original},i}$):

$$H_g = \frac{\delta_{\text{new},1}}{\delta_{\text{original},1}} = \frac{\delta_{\text{new},2}}{\delta_{\text{original},2}} = \frac{\delta_{\text{new},3}}{\delta_{\text{original},3}} \tag{15}$$

$$H_n = \frac{\delta_{\text{new},4}}{\delta_{\text{original},4}} = \frac{\delta_{\text{new},5}}{\delta_{\text{original},5}} = \frac{\delta_{\text{new},6}}{\delta_{\text{original},6}} = \frac{\delta_{\text{new},7}}{\delta_{\text{original},7}} \tag{16}$$

Therefore, a value of $H_g = 1$ and $H_n = 1$ represents the original confidence intervals reported in Table 1, while smaller values of H_g and H_n represent tighter confidence intervals. We are aware that this represents a simplifying assumption and that in a realistic setting (i.e., when additional experimental data is used for parameter estimation), the resulting confidence intervals would not all contract by the same factor. However, we believe that this simplification provides the merit of a reduction in dimensionality, which in turn enables a succinct analysis as shown below.

In Figure 5 we report how the "in spec" fraction of process outcomes, P_Y for the yield

and $P_{\overline{L}}$ for the mean particle size, changes for various values of H_g and H_n. Note that in these figures the top right corner corresponds to the original (wide) confidence intervals and therefore consequently reports a low fraction of "in spec" process outcomes in all cases, which agrees with the observations made in Figure 4. Considering Figures 5a and 5b ($\overline{L}_d = 200\mu$m, case I) in more detail, we see that shrinking the confidence intervals of the growth rate parameters (i.e., moving towards lower H_g) results in a considerable increase of P_Y and $P_{\overline{L}}$, while shrinking the confidence intervals of the nucleation rate parameters does not noticeably affect the fraction of "in spec" process outcomes. A similar situation can be identified in Figures 5c and 5d ($\overline{L}_d = 400\mu$m, case II), with the only noticeable difference being that H_n exhibits a stronger influence on $P_{\overline{L}}$, which can best be seen by the increase of $P_{\overline{L}}$ when moving towards lower H_n values at $H_g = 0.1$. Focussing now on the batch/PFC case with the same operating policies (Figure 6), we see that the batch/PFC case reinforces the previous observations, i.e., knowing the growth rate kinetics precisely is more beneficial than shrinking the confidence intervals on the nucleation rate parameters. However, the results for $P_{\overline{L}}$ remain unsatisfactory in the batch/PFC case with the exception of the lower left region of Figures 6a and 6c, which mirrors the results from the MSMPRC cascade (Figures 5a and 5c). For case I the batch/PFC shows a distinct advantage in comparison to the cascade of three MSMPRCs in terms of reaching the desired yield (cf. Figure 6b), i.e., the desired yield is already reached with a high probability using the original confidence intervals (which can also be seen from the red curve in Figure 4d), so that it cannot increase any further when tighter confidence intervals are presumed for any parameters. Note that while we have found similar behaviors in all cases (case I and II in the MSMRPC cascade and the batch/PFC case) when we only consider $P_{\overline{L}}$, we cannot claim that these observations will be valid for other substance systems since the kinetics will be different. Additionally, it bears mention that obtaining tighter confidence intervals on growth rate parameters can experimentally often be accomplished with relatively few experiments while a thorough characterization of the inherently stochastic phenomenon of nucleation is often laborious.

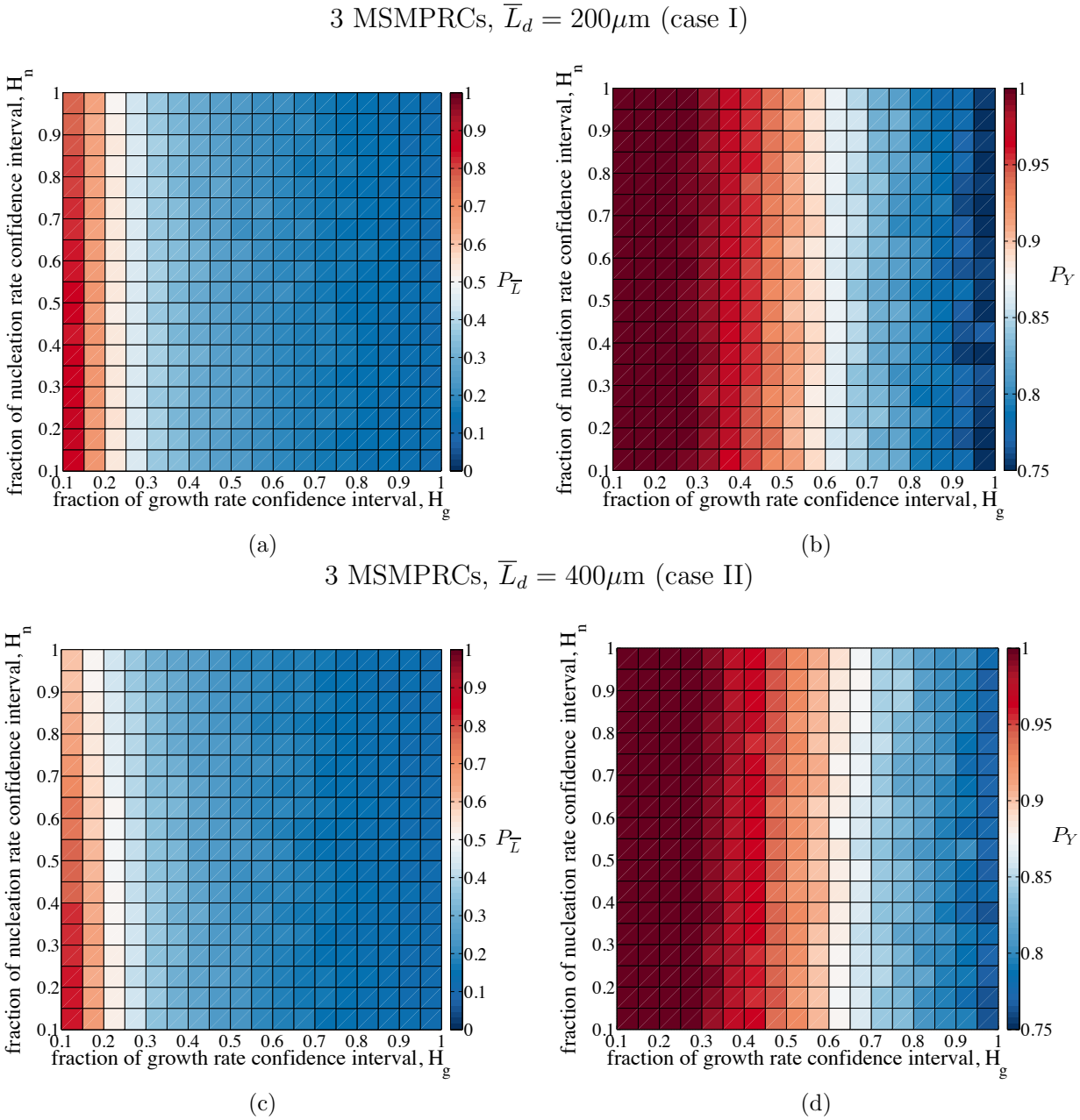

Figure 5: Influence of parameter uncertainty on process outcomes of a cascade of three MSMPRCs with total residence time $\tau = 2.75$ hours. The confidence intervals of the growth and nucleation parameters have been shrunk to a fraction of their original size (H_g and H_n, respectively). In all subfigures the color scale represents the probability that the mean particle size or the yield obtained are "in spec".

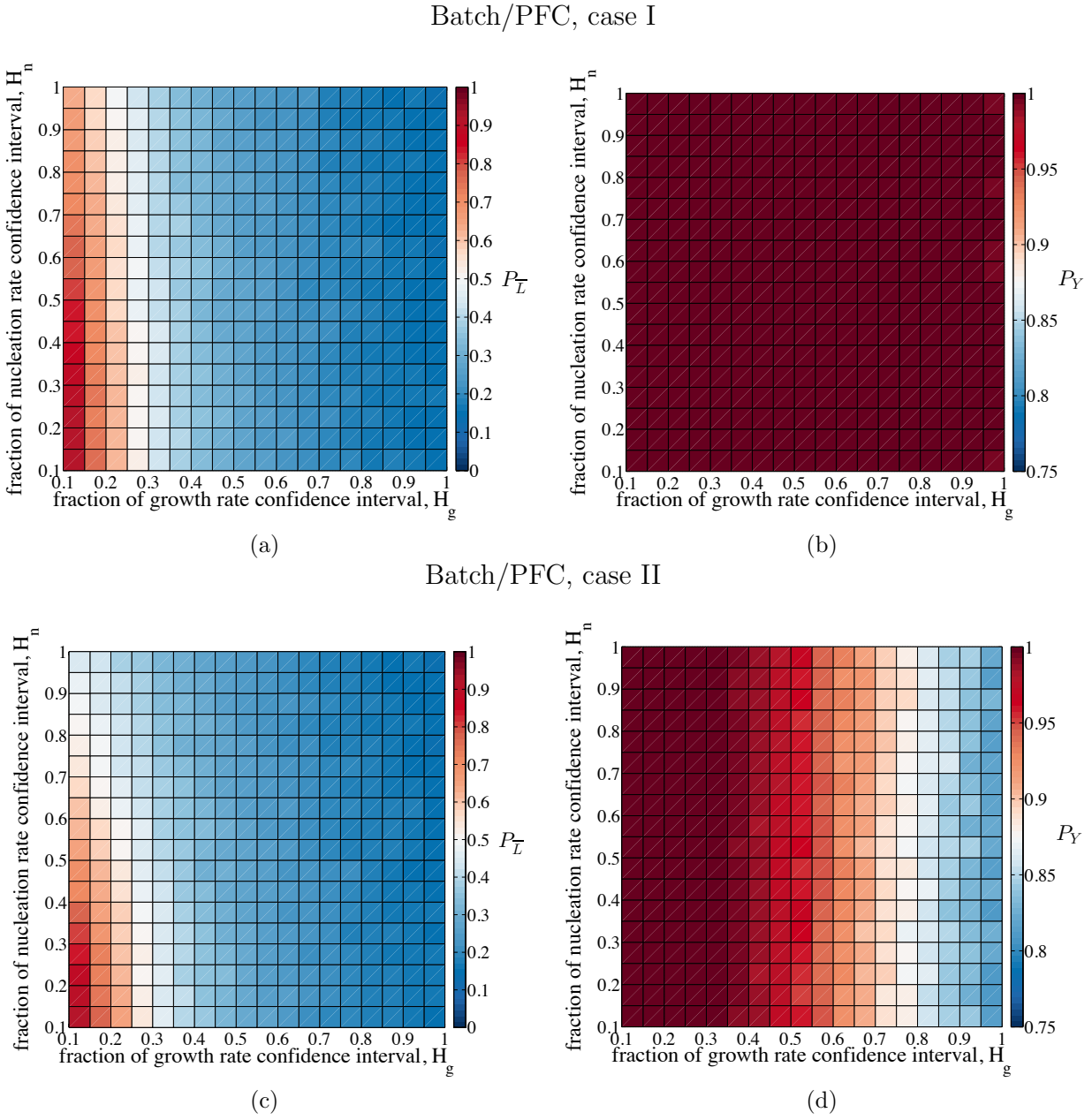

Figure 6: Influence of parameter uncertainty on process outcomes of the batch/PFC with total residence time $\tau = 2.75$ hours. The confidence intervals of the growth and nucleation parameters have been shrunk to a fraction of their original size (H_g and H_n, respectively). In all subfigures the color scale represents the probability that the mean particle size or the yield obtained are "in spec".

5.4 Uncertainty-adjusted attainable regions

Following the methodology presented in Section 4.2 we present uncertainty-adjusted attainable regions for some selected crystallizer configurations. We again sample the probability density function $g(\mathbf{k})$ and obtain a set of $N_s \times N_k$ kinetic parameters for which we calculate the attainable regions by solving Eq. (13) for various total residence times τ. We have chosen to sample $N_s = 500$ times and calculated the attainable region for total residence times τ between 1 and 10 hours with 50 discretization points. The resulting uncertainty-adjusted attainable regions for cascades consisting of two to five MSMPRCs are reported in Figure 7.[50] The colored surface in each subfigure represents the probability $p(\overline{L}, \tau)$ with which a specific point ($\overline{L}$,τ) can be attained and the black solid line represents the original attainable region obtained for the mean parameter values $\overline{\mathbf{k}}$. Note that for a given desired particle size, the points on the boundary of any of our attainable regions represent the process configurations with the lowest possible residence time, which in turn (for a given production rate) would result in the smallest possible equipment that satisfies the design specifications. However, when we consider the case of a cascade of two MSMPRCs (Figure 7a) we immediately notice that the points on the boundary of the original attainable region can be reached with a probability of less than 50%, which has strong implications on the way a crystallization process should be designed. In order to design a process that can reach the specifications with a high probability, it is ill-advised to consider process designs on the boundary of the attainable region. In fact, in order to design a robust process that fulfills the process specifications with a high probability, the uncertainty-adjusted attainable region indicates that higher residence times (i.e., larger equipment) should be considered, i.e., there exists a tradeoff between additional residence time (i.e., additional capital cost) and a more robust process design. For cascades with additional crystallizers (Figures 7b to 7d) the situation is similar, however, the more crystallizers are added to the cascade, the closer an acceptable level of probability comes to the boundary of the original attainable region. However, there clearly are diminishing returns visible, i.e., the improvement from two to three MSMRPCs in a cascade is

considerable, but the improvement from four to five MSMPRCs in the cascade is already significantly smaller. Adding crystallizers to the cascade corresponds to higher investment costs as well, so that we are facing a similar tradeoff as in the case with adding additional residence time to the process. When quantifying this tradeoff, further considerations, such as process complexity, automation efforts and an increased probability of equipment failure, should be included. Finally, we can investigate the uncertainty-adjusted attainable region in the batch/PFC case (Figure 8), which confirms the observations made for the MSMRPC cascades: we again see that the boundary of the original attainable region can hardly be reached in the case of large particle sizes.

These qualitative observations can be confirmed by investigating the area of the attainable region at a certain probability level. In Figure 9a, we report the area of the attainable region at a certain probability level normalized by the area of original attainable region for each of the four MSMPRC cascades. In this figure we see that the higher the number of MSMPRCs in the cascade the flatter the observed relationship between the relative area of the attainable region and the probability level becomes. Hence, this confirms our observation from the previous figure, where we have discovered that the effect of parameter uncertainty is less impactful for cascades with more MSMPRCs. This conclusion can be rationalized by realizing that a higher number of MSMPRCs also results in more process variables (temperatures, residence times), which can be used to counteract the effect of parameter uncertainty.

To quantify the influence of the width of the confidence intervals on this relationship, we report in Figure 9b the case of a cascade of three MSMPRCs where the confidence intervals are 50% and 25% of their original size (i.e., $H_g = H_n = 0.5$ and $H_g = H_n = 0.25$, respectively). The narrower the confidence interval, the flatter the curve becomes for intermediate probabilities. The observed behavior is consistent with the fact that perfectly known kinetics without any confidence intervals on them would result in a degenerated curve that is a point at (1,1) in this graph. The practical aspect of this observation is that an additional characterization of kinetics, which should result in more precisely known

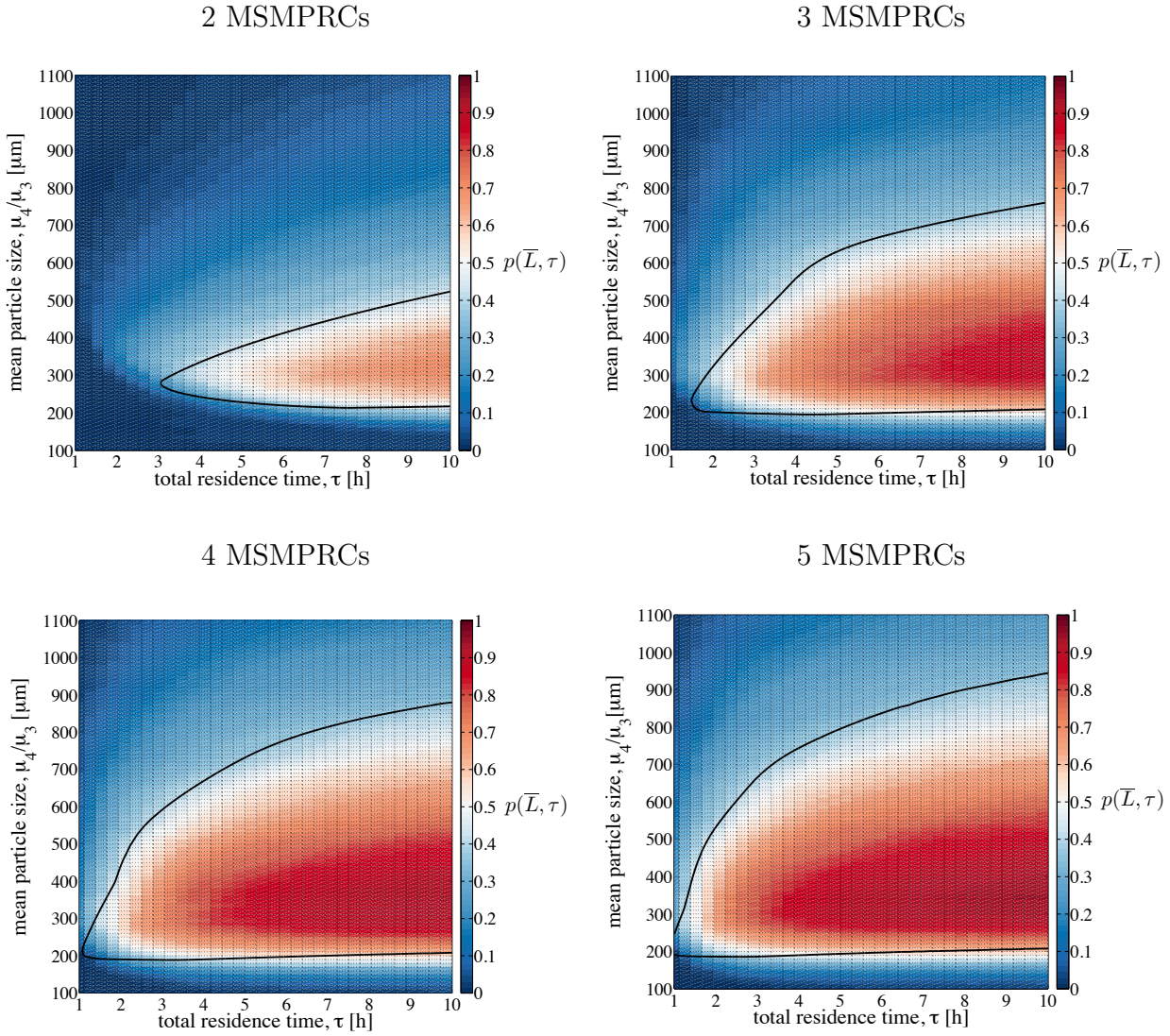

Figure 7: Uncertainty-adjusted attainable regions of particle size for cascades consisting of two to five MSMPRCs. The black solid line in each subfigure represents the attainable region obtained for the mean parameter values reported in Table 1.

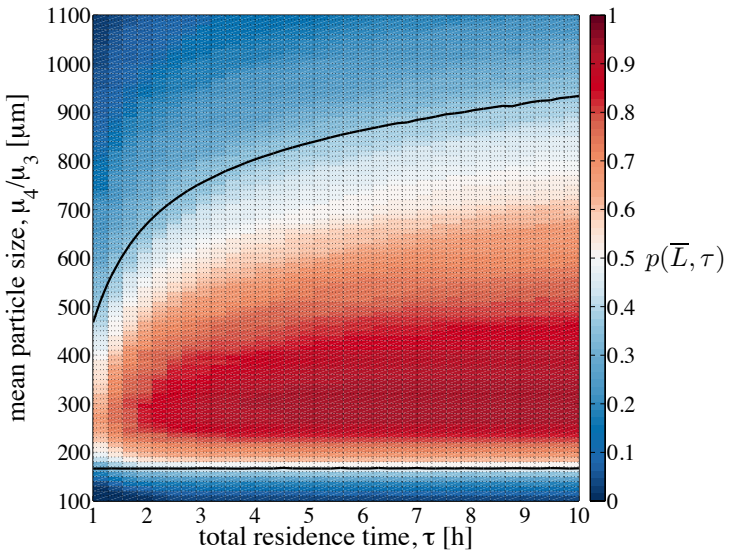

Figure 8: Uncertainty-adjusted attainable region for the batch/PFC case. The black solid line represents the attainable region obtained for the mean parameter values reported in Table 1.

kinetics, yields better defined attainable regions which can in turn be used to design robust crystallization processes that fulfill the design specifications with a high probability.

In summary, the concept of the uncertainty-adjusted attainable regions allows us to identify the tradeoffs between the desire for a robust process, investment costs and experimental effort invested in characterizing the crystallization kinetics.

6 Concluding Remarks

In this article we have investigated the influence of uncertainty in kinetic parameters on process outcomes. For the case study and the crystallizer configurations considered, we observed that the uncertainty present in kinetic parameters has significant effects on the yield and the mean particle size obtained from these processes, i.e., the distribution of process outcomes was rather wide in all cases and a considerable fraction of process outcomes would not fulfill the posed yield and size specifications. We have shown that this pertains to both batch and continuous crystallizers to a similar extent.

We then investigated if further characterization efforts should be focussed on improving

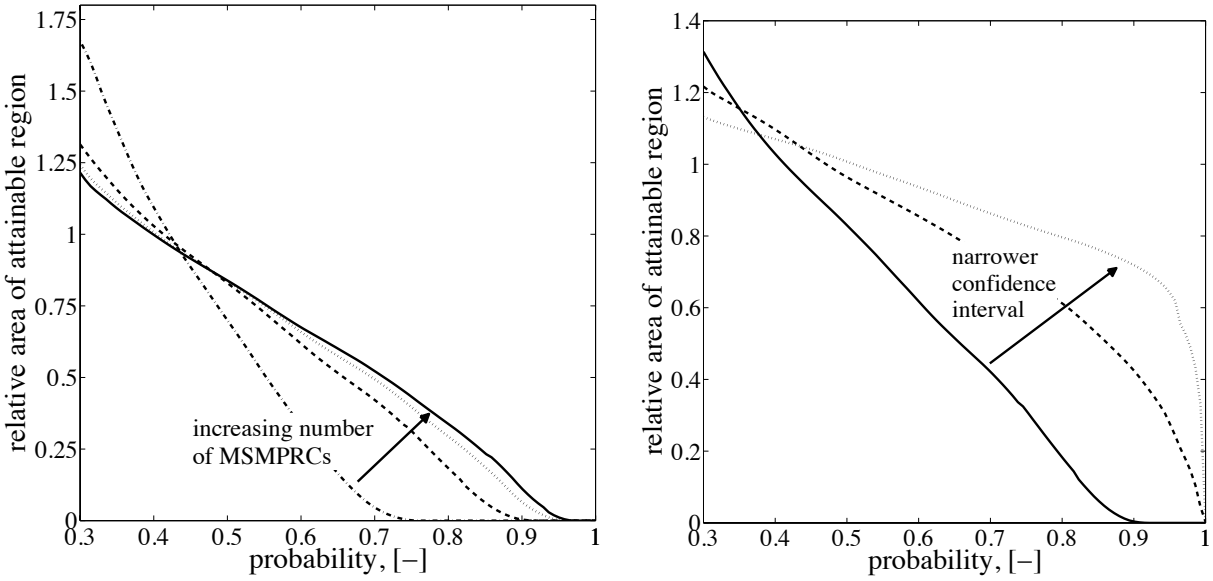

Figure 9: (a) Relative size of the attainable regions for different MSMPRC cascades (2 – 5 MSMPRCs); (b) Relative size of the attainable region for a cascade of 3 MSMPRCs for different confidence interval widths. Solid line: Original confidence intervals (cf. Table 1); dashed line: confidence interval width reduced to half for all parameters ($H_g = H_n = 0.5$); dotted line: confidence interval width reduced to a quarter for all parameters ($H_g = H_n = 0.25$).

the kinetic parameters in the growth rate or the kinetic parameters in the nucleation rate by shrinking the confidence interval for these kinetics individually. Hence, this analysis provides a fresh take on the age old question "Which is More Important for Achieving the Desired PSD: Nucleation Law or Growth Law?". While we have provided an answer to this question for the specific case study considered in this article (i.e., the growth rate is more important), we cannot claim that this answer will be generally applicable to all crystallization processes as the crystallization kinetics will be different. However, we believe that the presented Monte Carlo approach does help to target characterization efforts where they are most useful. This in turn should lead to faster development of robust crystallization processes.

We have shown how uncertainty-adjusted attainable regions can be obtained and how they can be used to design more robust processes. Staying away from regions of low probability ensures that the desired specifications can eventually be met when more data is obtained about the process. This is in contrast to designing the process in a low probability region (e.g., the boundary of the original attainable region), where the specifications can most likely not be met. However, the robustness gained in such a manner unfortunately comes at the price of higher investment costs associated with longer residence times, larger equipment and/or more crystallizers. We believe that the presented methodology could form the basis for evaluating and quantifying such tradeoffs and could thus enable an informed decision.

Supporting Information Available

We provide the model equations for the plug flow and semi-batch crystallizers, discuss the operating policies used in the case study in detail, and provide an example why mixing rules employed in attainable regions for chemical reactors might yield undesired results in particulate processes. This material is available free of charge via the Internet at `http://pubs.acs.org/`.

Acknowledgement

Research was supported in part by a Lilly Innovation Fellowship Award to TV from Eli Lilly and Company. TV and MFD thank Prof. Antonis Kokossis for helpful discussions about attainable regions that occurred during the "Foundations of Computer Aided Process Design" conference held in Cle Elum, WA, July 2014.

Notation

Roman letters		
a	weight fraction (solute free basis) of anti-solvent	[-]
c	solute concentration (solute free basis)	[kg m^{-3}]
$c_\star(T,a)$	solubility	[kg m^{-3}]
$\mathcal{C}$	parameter confidence region	[varies]
$f(z)$	volumetric flow rate differential anti-solvent differential side stream to PFC	[m^2 s^{-1}]
F_i	volumetric flow rate of anti-solvent stream to i^{th} MSMPRC	[m^3 s^{-1}]
$F(t)$	volumetric flow rate of anti-solvent stream to semi-batch crystallizer	[m^3 s^{-1}]
$g(\mathbf{k})$	probability density function of the parameters	[varies]
G	crystal growth rate	[m s^{-1}]
H_g	fraction of original confidence intervals of growth rate parameters	[-]
H_n	fraction of original confidence intervals of nucleation rate parameters	[-]
J	nucleation rate	[m^{-3} s^{-1}]
k_v	volumetric shape factor	[-]
k_i	kinetic parameters	[varies]
$\mathbf{k}$	vector of kinetic parameters	[varies]
$\overline{\mathbf{k}}$	vector of mean parameter values	[varies]
L	crystal size	[m]
$\overline{L}$	volume weighted mean particle size, μ_4/μ_3	[m]
$\overline{L}_d$	desired volume weighted mean particle size	[m]
m	number of MSMPRCs in the cascade	[-]
n	number density distribution	[m^{-4}]
N_k	number of kinetic parameters	[-]
N_s	number of samples used in the Monte Carlo procedure	[-]
p_Y	probability density function of process yield	[-]
$p_{\overline{L}}$	probability density function of volume-weighted mean particle size at the end of the process	[m^{-1}]
$p(\tau,\overline{L})$	probability that particles of mean size $\overline{L}$ is attainable at total residence time τ	[-]
P	production rate	[kg s^{-1}]
P_Y	fraction of process outcomes within yield tolerance	[-]

$P_{\overline{L}}$	fraction of process outcomes with mean sizes within tolerance	[-]
Q	volumetric flow rate	[$m^3 s^{-1}$]
R	length of PFC	[m]
S	supersaturation	[-]
t	time	[s]
$t_{\alpha,\nu}$	quantile of Student's t distribution with confidence level α and degrees of freedom ν	[-]
T	temperature	[K]
V	volume of suspension	[m^3]
$\mathbf{V}_k$	parameter covariance matrix	[varies]
Y	fraction of attainable yield	[-]
Y_d	desired yield	[-]
z	length coordinate along PFC	[m]
Z	length of PFC	[m]

Greek letters

α	confidence level	[-]
δ_i	confidence interval of parameter i with confidence level α	[varies]
$\delta\left(\mathbf{k}-\overline{\mathbf{k}}\right)$	Dirac delta distribution	[varies]
ϵ_Y	yield tolerance	[-]
$\epsilon_{\overline{L},\ell}$	tolerance on lower size limit	[m]
$\epsilon_{\overline{L},h}$	tolerance on upper size limit	[m]
τ	total residence time in MSMPRC cascade, PFC or semi-batch crystallizer	[s]
τ_i	residence time in i^{th} MSMPRC	[s]
ρ_c	crystal density	[kg m^{-3}]
μ_j	j^{th} moment of number density distribution	[kg m^{j-3}]
ν	degrees of freedom of Student's t distribution	[-]
Φ	objective function in parameter estimation procedure	[varies]

Notes and References

(1) Liu, Y.; Yin, H.; Yuan, S.; Chen, Z. Influence of particle characteristics and E/Z-isomer ratio on the colour of concentrated β-carotene dispersions. *Int. J. Food. Sci. Tech.* **2010**, *45*, 1450–1456.

(2) Rasenack, N.; Müller, B. Ibuprofen crystals with optimized properties. *Int. J. Pharm.* **2002**, *245*, 9–24.

(3) Variankaval, N.; Cote, A.; Doherty, M. From form to function: Crystallization of active pharmaceutical ingredients. *AIChE J.* **2008**, *54*, 1682–1688.

(4) Brazeau, G.; Sauberan, S.; L, G.; Wisniecki, P.; Shah, J. Effect of particle size of parenteral suspensions on in vitro muscle damage. *Pharm. Dev. Technol.* **2011**, *16*, 591–598.

(5) Nagy, Z.; Braatz, R. Advances and New Directions in Crystallization Control. *Annu. Rev. Chem. Biomol. Eng.* **2012**, *3*, 55–75.

(6) Doki, N.; Kubota, N.; Sato, A.; Yokota, M. Effect of cooling mode on product crystal size in seeded batch crystallization of potassium alum. *Chem. Eng. J.* **2001**, *81*, 313–316.

(7) Worlitschek, J.; Mazzotti, M. Model-based optimization of particle size distribution in batch-cooling crystallization of paracetamol. *Cryst. Growth Des.* **2003**, *3*, 891–903.

(8) Ward, J.; Mellichamp, D.; Doherty, M. Choosing an operating policy for seeded batch crystallization. *AIChE J.* **2006**, *52*, 2046–2054.

(9) Corriou, J.; Rohani, S. A new look at optimal control of a batch crystallizer. *AIChE J.* **2008**, *54*, 3188–3206.

(10) Aamir, E.; Nagy, Z.; Rielly, C. Optimal seed recipe design for crystal size distribution control for batch cooling crystallization processes. *Chem. Eng. Sci.* **2010**, *65*, 3602–3614.

(11) Seki, M.; Furuya, N.; Hoshino, S. Evalutation of controlled cooling for seeded batch crystallization incorporating dissolution. *Chem. Eng. Sci.* **2012**, *77*, 10–17.

(12) Fujiwara, M.; Chos, P.; Ma, D.; Braatz, R. Paracetamol crystallization using laser backscattering and ATR-FTIR spectroscopy: metastability, agglomeration, and control. *Cryst. Growth Des.* **2002**, *2*, 363–370.

(13) Chew, J.; Chos, P.; Tan, R. Automated in-lin technique using FBRM to achieve consistent product quality in cooling crystallization. *Cryst. Growth Des.* **2007**, *7*, 830–838.

(14) Mesbah, A.; Huesman, A.; Kramer, H.; Van den Hof, P. Real-time control of industrial batch crystallization processes using a population balance modeling framework. *AIChE J.* **2011**, *57*, 1557–1569.

(15) Saleemi, A.; Rielly, C.; Nagy, Z. K. Automated direct nucleation control for in situ dynamic fines removal in batch cooling crystallization. *CrystEngComm* **2012**, *14*, 2196–2203.

(16) Ma, D.; Chung, S.; Braatz, R. Worst-case performance analysis of optimal batch control trajectories. *AIChE J.* **1999**, *46*, 1469–1476.

(17) Nagy, Z.; Braatz, R. Robust Nonlinear Model Predictive Control of Batch Processes. *AIChE J.* **2003**, *49*, 1776–1786.

(18) Nagy, Z.; Braatz, R. Open-loop and closed-loop robust optimal control of batch processes using distributional and worst-case analysis. *J. Process Contr.* **2004**, *14*, 411–422.

(19) Nagy, Z. Model based robust control approach for batch crystallization product design. *Comput. Chem. Eng.* **2009**, *33*, 1685–1691.

(20) Castagnoli, C.; Yahyah, M.; Cimarosti, Z.; Peterson, J. Application of Quality by Design Principles for the Definition of a Robust Crystallizaton process for Casopitant Mesylate. *Org. Process Res. Dev.* **2010**, *14*, 1407–1419.

(21) Samad, N.; Sin, G.; Gernaey, K.; Gani, R. Introducing uncertainty analysis of nucleation and crystal growth models in Process Analytical Technology (PAT) system design of crystallization processes. *Eur. J. Pharm. Biopharm.* **2013**, *85*, 911–929.

(22) Nagy, Z.; Braatz, R. Worst-case and distributional robustness analysis of finite-time control trajectories for nonlinear distributed parameter systems. *IEEE Trans. Control Syst. Technol.* **2003**, *11*, 1694–704.

(23) Rawlings, J.; Miller, S.; Witkowski, W. Model Identification and Control of Solution Crystallization Processes: A Review. *Ind. Eng. Chem. Res.* **1993**, *32*, 1275–1296.

(24) Vetter, T.; Burcham, C.; Doherty, M. Regions of attainable particle sizes in continuous and batch crystallization processes. *Chem. Eng. Sci.* **2014**, *106*, 167–180.

(25) Levenspiel, O. *Chemical Reaction Engineering*, 3rd ed.; John Wiley & Sons: Hoboken, NJ, 1999.

(26) Ramkrishna, D. *Population Balances: Theory and Applications to Particulate Systems in Engineering*; Academic Press: San Diego, 2000.

(27) Randolph, A. D.; Larson, M. A. *Theory of Particulate Process: Analysis and Techniques of Continuous Crystallization*, 2nd ed.; Academic Press: New York, 1988.

(28) Chen, B. H.; Asprey, S. On the Design of Optimally Informative Dynamic Experiments for Model Discrimination in Multiresponse Nonlinear Situations. *Ind. Eng. Chem. Res.* **2003**, *42*, 1379–1390.

(29) Chen, B.; Bermingham, S.; Neumann, A.; Kramer, H.; Asprey, S. On the Design of Optimally Informative Experiments for Dynamic Crystallization Process Modeling. *Ind. Eng. Chem. Res.* **2004**, *43*, 4889–4902.

(30) Cooney, M. J.; McDonald, K. A. Optimal Dynamic Experiments for Bioreactor Model Discrimination. *Appl. Microbiol. Biotechnol.* **1995**, *43*, 826–837.

(31) Bard, Y. *Nonlinear Parameter Estimation*; Academic Press: New York, 1974.

(32) Caracotsios, M.; Stewart, W. E. Sensitivity Analysis of Initial Value Problems with Mixed ODEs and Algeraic Equations. *Comp. Chem. Eng.* **1985**, *9*, 359–365.

(33) Donaldson, J. R.; Schnabel, R. B. Computational Experience with Confidence Regions and Confidence Intervals for Nonlinear Least Squares. *Technometrics* **1987**, *29*, 67–82.

(34) Nagy, Z.; Braatz, R. Distributional uncertainty analysis using power series and polynomial chaos expansions. *J. Process Contr.* **2007**, *17*, 229–240.

(35) Horn, F. Attainable and Non-Attainable Regions in Chemical Reaction Technique. *In Proceedings of the Third European Symposium on Chemical Reaction Engineering* **1964**, 293.

(36) Glasser, D.; Hildebrandt, D.; Crowe, C. A Geometric Approach to Steady Flow Reactors: The Attainable Region and Optimization in Concentration Space. *Ind. Eng. Chem. Res.* **1987**, *26*, 1803–1810.

(37) Hildebrandt, D.; Glasser, D.; Crowe, C. Geometry of the Attainable Region Generated by Reaction and Mixing: With and without Constraints. *Ind. Eng. Chem. Res.* **1990**, *29*, 49–58.

(38) Nisoli, A.; Malone, M. F.; Doherty, M. F. Attainable Regions for Reaction with Separation. *AIChE J.* **1997**, *43*, 374–387.

(39) Feinberg, M.; Hildebrandt, D. Optimal reactor design from a geometric viewpoint I. Universal properties of the attainable region. *Chem. Eng. Sci.* **1997**, *62*, 1637–1665.

(40) Feinberg, M. Toward a theory of process synthesis. *Ind. Eng. Chem. Res.* **2002**, *41*, 3751–3761.

(41) Tang, Y.; Feinberg, M. Carnot-like Limits to Steady-State Productivity. *Ind. Eng. Chem. Res.* **2007**, *46*, 5624–5630.

(42) Note that we write "modified" because mixing rules used in attainable regions for chemical reactors and mixers should not readily be extended to particulate processes; the interested reader is referred to the Supporting Information (Appendix C) for details.

(43) Raikar, N. B. Prediction And Manipulation Of Drop Size Distribution Of Emulsions Using Population Balance Equation Models For High-Pressure Homogenization. Ph.D. thesis, University of Massachusetts – Amherst, 2010.

(44) Ridder, B.; Majumder, A.; Nagy, Z. Population Balance Model-Based Multiobjective Optimization of a Multisegment Multiaddition (MSMA) Continuous Plug-Flow Antisolvent Crystallizer. *Ind. Eng. Chem. Res.* **2014**, *53*, 4387–4397.

(45) Mitchell, N. A.; Ó'Ciardhá, C. T.; Frawley, P. J. Estimation of the growth kinetics for the cooling crystallisation of paracetamol and ethanol solutions. *J. Cryst. Growth* **2011**, *328*, 39–49.

(46) Mitchell, N. A.; Frawley, P. J.; Ó'Ciardhá, C. T. Nucleation kinetics of paracetamol-ethanol solutions from induction time experiments using Lasentec FBRM. *J. Cryst. Growth* **2011**, *321*, 91–99.

(47) Frawley, P. J.; Mitchell, N. A.; Ó'Ciardhá, C. T.; Hutton, K. W. The effects of supersaturation, temperature, agitation and seed surface area on the secondary nucleation of paracetamol in ethanol solutions. *Chem. Eng. Sci.* **2012**, *78*, 183–197.

(48) Codan, L.; Eckstein, C.; Mazzotti, M. Growth Kinetics of S-Mandelic Acid in Aqueous Solutions in the Presence of R-Mandelic Acid. *Cryst. Growth Des.* **2013**, *13*, 652–663.

(49) Vetter, T.; Mazzotti, M.; Brozio, J. Slowing the growth rate of ibuprofen crystals using the polymeric additive Pluronic F127. *Cryst. Growth Des.* **2011**, *11*, 3813–3821.

(50) Obtaining one such uncertainty-adjusted attainable region takes roughly $N_s \times 5$ minutes on a 3.4 Ghz quad-core Intel Core i7-4770 processor with 8 GB working memory with a frequency of 800 MHz. Note that the calculation time scales linearly with the number of cores involved, since the calculations are easily parallelized.

For table of contents use only:

This graphic is intended for table of content use.